Ocean Engineering 317 (2025) 119983

Contents lists available at ScienceDirect

Ocean Engineering

journal homepage: www.elsevier.com/locate/oceaneng

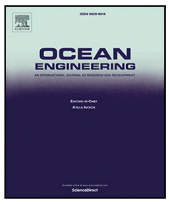

Research paper

# Performance evaluation of point-absorber wave energy converters; energy extraction and structural integrity aspects

Mohammad Mahdi Abaei [a,b], Ehsan Arzaghi [c], Minghan Bao [a,b], Vikram Garaniya [d,e], Nagi Abdussamie [f], Alexandre Pichard [g], Rouzbeh Abbassi [a,*]

[a] School of Engineering, Faculty of Science and Engineering, Macquarie University, Sydney, NSW, Australia
[b] Blue Economy Cooperative Research Centre, Launceston, TAS, Australia
[c] School of Mechanical, Medical and Process Engineering, Faculty of Engineering, Queensland University of Technology, Brisbane, QLD, Australia
[d] Australian Maritime College, University of Tasmania, Launceston, TAS, Australia
[e] Department of Chemical and Environmental Engineering, School of Engineering, STEM College, RMIT University, Melbourne, VIC, Australia
[f] University of Doha for Science and Technology, Doha, Qatar
[g] Carnegie Clean Energy, Fremantle, WA, Australia

ARTICLE INFO

*Keywords:*
Blue economy
Offshore renewable energy systems
Point-absorber
Wave energy converter
Fatigue
Bayesian statistics

ABSTRACT

Offshore aquaculture industries face significant challenges in securing reliable and environmentally friendly energy sources. Among the possible solutions, wave energy converters (WECs) show a promising solution to transfer the technology for creating sustainable operations for remotely accessible fish farms. However, ideally integrating them into the aquaculture floating vessels necessitates a careful and thorough design approach. This paper presents a comprehensive framework for evaluating the performance of the AquaPower platform (APP) concept vessel in supporting offshore fish farm operations. Drawing inspiration from established WEC principles, this concept merges a floating platform with a tensioned mooring lines integrated with power take off systems connected to a moored vessel. The framework addresses crucial aspects, including power generation, structural resilience, and mitigation of mooring fatigue-induced deterioration, which are essential for optimizing the APP's performance. To enhance evaluation the reliability of the structure, the framework introduces a robust surrogate model based on Bayesian data analysis. This enables the assessment of mooring asset reliability and projected lifespan for real-time monitoring. The practical demonstration of this framework investigated through a case study for designing and evaluating the APP, effectively highlighting its potential as a feasible wave energy solution for the progress of offshore aquaculture towards blue economy technology. This paper's primary aim is to contribute to affirming the feasibility and viability of the APP concept as an effective and sustainable wave energy remedy for offshore aquaculture. The results of this study can be applied to other contexts, demonstrating the framework's ability to enhance the dependability of various offshore energy structures, including floating wind turbines, and extend their operational lifespan.

## 1. Introduction

With the expected increase in the global population to 9 billion by 2050, management of the food and energy nexus is of significant importance (FAO, 2017). Moving aquaculture operation to offshore locations presents numerous benefits, including access to abundant resources, reduced conflict with stakeholders, and enhanced environmental sustainability. Seafood production involves several energy-intensive activities, like feeding with barge vessels, which heavily rely on diesel generators. This reliance results in significant costs, caused by volatility of the fossil fuel prices, and detrimental effects to the (marine) environment. Energy production form offshore renewable resources can offer an opportunity to make future aquaculture developments and the associated offshore industries more sustainable. Major offshore renewable energy systems (ORESs) include wind and wave technologies. Wave energy is a predictable resource with higher power per unit area of 2–3 $kW/m^2$ than wind (0.4–0.6 $kW/m^2$) and less intermittency compared to all other offshore renewables (Kumar et al., 2023).

In addition to the substantial available resources, the technologies used to extract wave energy can offer several advantages over offshore wind turbines. For instance, wave energy converters (WECs) are easier to install compared to offshore wind turbines due to their smaller size and simpler structures. They also have fewer critical components,

* Corresponding author.
*E-mail address:* Rouzbeh.Abbassi@mq.edu.au (R. Abbassi).

https://doi.org/10.1016/j.oceaneng.2024.119983
Received 23 July 2024; Received in revised form 1 November 2024; Accepted 28 November 2024
Available online 13 December 2024

specially those subject to large winds, increasing their capability to withstand extreme conditions in the marine environment. Over the past decade, a substantial body of research and development has been devoted to exploring a wide range of WEC concepts, including oscillating bodies, oscillating water column (OWC) and overtopping devices. Zhang et al. (2021) provides an extensive review of the technical principles of developed WEC concepts, reflecting the evolution of the field. In planning for future offshore developments, selecting an optimal design concept for introducing WEC technology into the aquaculture facilities will present significant engineering and operational challenges. This is due to several conditions inherent to the ocean environment, including extreme loads, structural deterioration caused by seawater and cyclic loads, site accessibility for repair and maintenance, and the lack of design convergence which has resulted in lower maturity of wave energy converters (Clemente et al., 2021). An integrated approach to infrastructure planning and design is needed, both in terms of WEC concept development and deployment to identify niche markets where competition and requirements are less demanding (Clemente et al., 2023). Such an approach must carefully give consideration to the important aspects of asset life cycle which could be optimized during the design process.

WEC technologies may provide a suitable solution to meet the energy demand and sustainability goals of the existing or future offshore industries such as the aquaculture sector. In reviewing major WEC concepts developed, it is conceptualized that some point absorber WECs may be suitable for integration with the offshore aquaculture facilities. In particular, installing WECs in the vicinity of aquaculture infrastructure can supply the substantial energy demand associated with the multi KW generators that support the vessels and crew operations. WEC farms can also provide a shield to aquaculture systems potentially enhancing their integrity and service life (Silva et al., 2018). A report by Freeman et al. (2022) provides a detailed view into offshore aquaculture as a market for ORES by identifying the technologies that can be adopted, opportunities and challenges, and recommendations to advance for ORES-aquaculture system co-location. Amongst the reviewed concepts, MoorPower, developed by Carnegie Clean Energy based on the design principles of Carnegie's CETO WEC, aims to replace the diesel generators used in aquaculture vessels including feed barges (Carnegie Clean Energy, 2022). The concept of utilizing similar power capture components like CETO on aquaculture vessels, where vessel motion is converted to electricity using power take-off (PTO) systems, offers technological transferability at lower costs. This could offer an attractive niche market for ORES; however, careful design process and additional operational experience are required to ensure reliability levels are consistent with those of operating aquaculture facilities. These challenges are mainly attributed to the complex interaction between the station-keeping systems and PTOs.

The complex hydrodynamic performance of floating vessel which is turned into a WEC (by adding PTOs) necessitates advanced modeling and simulation to develop an understanding of their motion characteristics, evaluate the system efficiency in energy extraction and to predict the reliability of the assets with regard to structural integrity. This is required to identify innovative technologies and design approaches that realize optimal performance and safety. It is important to note that the mooring lines and PTO systems are both subject to extreme loads and long-term structural deterioration processes including fatigue which can be exacerbated by unforeseen hydrodynamic loads. Assessment of fatigue damage accumulation in mooring lines of WECs is previously addressed by several standards and researchers (Davidson and Ringwood, 2017). Thies et al. (2014) developed a methodology in which numerical approaches are employed on experimental observations to predict mooring line fatigue at a design stage. This study used the observations from a generic WEC buoy with three-leg catenary rope-chain mooring, and does not account for the effect of PTO systems. To ensure a robust mooring design and survivability in the marine environment, the occurrence of extreme loads on WEC must be carefully evaluated as well.

To address these challenges, researchers have explored various mooring solutions. Previous studies show that taut moorings outperform slack moorings in certain wave energy converter (WEC) designs. For instance, Guo et al. (2017) found that a tautly moored floating breakwater effectively reduces wave impact at a set sea level, while a slackly moored one adapts better to tides. Customizing mooring setup based on WEC type and considering factors like environmental conditions and wave loads is vital. DNV (2010) offers guidance for modeling, analyzing, and predicting these conditions, along with calculating structural environmental loads. Studies conducted by Pillai et al. (2011) and Ringsberg et al. (2012) have presented approaches using optimization algorithms and experimental analyses to define optimum mooring layouts and to minimize the risks of failure due to structural degradation and extreme loads.

To the best of the authors' knowledge, a probabilistic framework to assess mooring and PTO design performance – specifically for co-located, multi-purpose offshore systems – has yet to be established. Existing studies have primarily focused on single-purpose offshore structures, leaving a critical gap in evaluating integrated systems that combine multiple mechanical devices within a single platform. Such floating systems, which merge WECs and civil structures such as aquaculture or offshore wind, demand unique considerations due to the complex and dynamic load interactions between system components. A robust framework for their design evaluation must address the long-term operational reliability and efficiency of both mooring and PTO subsystems, considering the major aspects of operation in harsh and energy-dense environment. The primary knowledge gap lies in the stochastic modeling of mooring and PTO elements in terms of their ability to harness maximum available energy while sustaining structural integrity. This gap is combined by the limited availability of experimental data to assess real-world power output and structural damage. Integration of hydrodynamic models with advanced statistical methods, which reduce dependence on large-scale data inputs, are critical for predicting system power output, failure probability, and overall platform resilience.

This paper presents a new probabilistic framework for performance evaluation of WECs with regard to power generation and structural reliability. The focus of the framework is moored point-absorber WECs, in particular the AquaPower Platform (APP) Concept which is introduced in the next section. The primary motivation for adopting the APP concept is twofold: to assess its effectiveness in energy harvesting using reactive mooring systems, and to enhance the vessel's survivability in extreme weather conditions through motion damping. To estimate the energy extraction capacity, a dynamic numerical approach is taken to modeling the hydrodynamic characteristics of the structure. A robust surrogate model based on Bayesian statistics is introduced to evaluate the fatigue deterioration in WECs. The surrogate model assesses how the most critical WEC components, mooring lines and PTOs, respond to the environment, and estimates failure probabilities based on structural reliability principles. This approach is significantly more efficient compared to other conventional solution methods. The application of the proposed framework is demonstrated through a case study of APP concept, providing valuable information into the feasibility of integrating wave energy systems with vessels supporting the offshore industries. The insights gained from this research have broader impact on enhancing the design performance of future ORESs.

The remainder of the work is structured as follows: Section 2 provides an introduction to the AquaPower Platform concept; Section 3 presents the integrated methodology developed for hydrodynamic analysis of ORES for power output estimation; Section 4 details the developed surrogate model for structural reliability analysis. Section 5 presents the application of the developed model through a case study involving the APP, including the results and discussion. Section 6 presents the concluding remarks of this paper and future research directions.

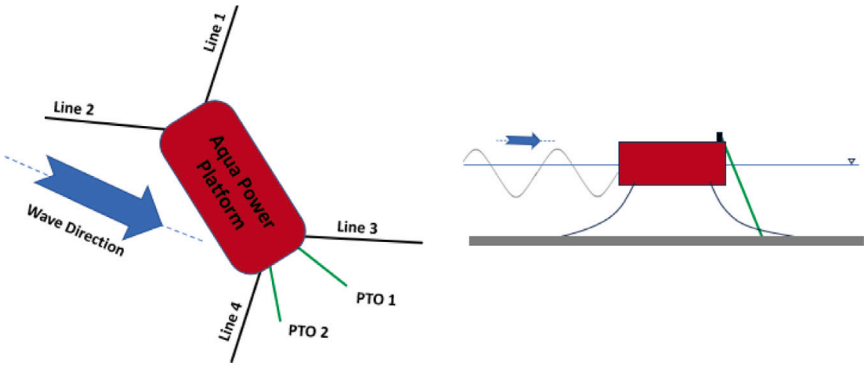


**Fig. 1.** The AquaPower WEC concept: - top view (left) shows the studied mooring/PTO arrangement, and side view (right) shows partial submergence of WEC buoy, and mooring/PTO geometries.

## 2. The AquaPower platform (APP) concept

Over the last decade, a large number of WEC concepts have emerged globally, each with unique strengths and limitations. The CETO WEC developed by Carnegie Clean Energy (Carnegie Clean Energy, 2022), is an innovative technology that utilizes submerged buoys tethered to seabed. The buoys move in all degrees of motion (due to having 3 moorings), running on-board rotary electrical PTOs to generate electricity. CETO has demonstrated promising results in small-scale deployments (Al Shami et al., 2023).

The APP concept in this paper is based on the MoorPower technology, which is an extension of the CETO concept for large-scale offshore aquaculture applications (Carnegie Clean Energy, 2022). Given that the detailed system architecture of MoorPower cannot be publicly published, a generic system architecture (shown in Fig. 1 is used for this work. Thus the performance and characteristics computed in this paper are not representatives of those of MoorPower. The APP concept is a representative of advanced co-located ORES systems where WEC units integrated into marine vessels for harnessing the kinetic energy from ocean waves. Although the marine vessels can vary in hull form and size, depending on their applications, a generic hull with block coefficient of 0.8 is selected for the numerical simulations within the present study to a step towards decarbonization of aquaculture operations with substantial demand for electricity. A schematic of the components within an APP structure and their arrangement is illustrated in Fig. 1. The floating structure is Supported by four mooring lines labeled Line 1–4, enabling the vessel to counteract the forces experienced from the environment to remain stable while producing electricity. Particularly, the aft mooring lines (3 & 4) are responsible to support the integrity of the PTO units facilitating energy extraction from vessel motions. The model includes two PTO units, labeled PT01-2. Understanding the dynamic responses of the system is an critical step towards optimizing its design for maximizing energy extraction, stability assurance, and mitigation of failures caused by extreme loads and fatigue.

Detailed probabilistic dynamic response analyses compromise evaluating the likelihood of the system withstanding varying sea states, extreme weather encounters and environmental factors. Such investigation ensures that the design functions effectively and reliably for wave energy extraction.

In the following sections, this study will introduce the theoretical framework which models the hydrodynamics of the APP concept and evaluates its performance. By analyzing and simulating the concept, the framework aims to offer valuable insights into its operational characteristics, and identify design improvement opportunities for enhanced reliability and energy efficiency.

## 3. Integrated dynamic analysis of floating power systems

To evaluate the APP's performance and identify the safe design configuration for extracting maximum wave energy, a crucial step is to model the system dynamics as an integrated body. This approach involves the physics of the floating structure in a random sea condition considering the flexible components, such as the mooring lines and PTO systems. Numerical models are utilized to compute the power matrices based on the time-domain responses of PTOs, obtained from comprehensive analyses of the interactions between the waves and APP. This model integrates the coupled non-linear equation of motion as described below (Babarit et al., 2012):

$$(M+\mu_\infty)\ddot{X} = F_{ex} - \int_0^t K(t-s)\dot{X}(s)ds + F_H + F_{PTO} + F_V + F_M + F_2, \quad (1)$$

where $X$, $\dot{X}$, and $\ddot{X}$ are the position, velocity, and acceleration of the structure, respectively. To account for the degree of freedom (DoF), these parameters are considered as matrices with the number of rows equal to the DoF. The matrix corresponding to device mass, denoted as $M$, is not necessarily constant and depends on the added mass incurred by device (frequency dependent). Thus the parameter $M$ can be a function of the position and velocity vectors $X$ and $\dot{X}$, especially when the object has larger responses causing variations in its buoyancy. $F_{ex}$ is the first-order wave excitation force, which significantly contributes to the environmental loads on the floater. Additionally, $\mu_\infty$ and $K(t)$ denote the added mass matrix at high frequency and the memory function of the radiation forces, respectively. These quantities estimate the frequency-dependent added mass and hydrodynamic damping. $F_H$ represents the hydrostatic force resulting from the combined action of gravity and buoyancy. $F_{PTO}$ is the force applied by the PTO system, which requires detailed modeling to capture the effects of the complex control force strategy used for wave power extraction. $F_V$ is the damping force, which varies quadratically with velocity to incorporate the effect of viscous losses. $F_M$ is the mooring force modeled using an elastic Finite Element Method (FEM) in this study, similar to the approach used for PTO modeling. The hydrodynamic loads on the flexible mooring and PTO lines are estimated using the Morison equation. $F_2$ is the force corresponding to the non-linear terms of the second-order hydrodynamic loads in the equation of motion. This force is caused by wave drift and sum frequency. Although the contributions of these non-linear loads are smaller compared to the first-order loads, their inclusion is crucial to obtaining a more accurate estimation of the structure modal shapes and natural period which directly affects the response of mooring lines and PTOs. This is particularly important in the presence of higher-order wave components.

In this study, the potential flow theory was employed to model waves and wave-structure interactions. While this theory generally aligns well with experiments in small to moderate sea states, it may lead to discrepancies in severe sea states or under resonant wave conditions due to non-linear and/or viscous effects, resulting in an overestimation of dynamic response and energy absorption. Several studies have previously adopted this approach for estimating the expected power extraction during the design process of marine energy systems, although

agreeing it provides upper estimates (Bånkestad, 2013; Faraggiana et al., 2022; Babarit et al., 2012). The Boundary Element Method (BEM) has been employed using the Orcawave commercial software package as a powerful numerical technique for computing the excitation loads ($F_{ex}$). BEM offers notable advantages in capturing wave-body interactions including accuracy and computational efficiency which allows for precise determination of the wave exciting force.

The same governing equation is revisited to calculate the radiation loads - a significant contributor to the frequency-dependent added mass and damping components of the hydrodynamic loads. Boundary conditions are imposed to account for the oscillation of fluid particles near the floating body at the frequency of the incident wave. It should be noted that the integral term in Eq. (1) represents the hydrodynamic radiation force in the frequency domain. The relationship for this force can be simplified as $\tau_{\text{rad}} = -B(\omega)\dot{X} - A(\omega)\ddot{X}$, where $A(\omega)$ and $B(\omega)$ are frequency-dependent symmetric matrices for added mass and damping, respectively, and $\dot{X}$ and $\ddot{X}$ are the generalized velocity and acceleration vectors of the floating body motions. It is known that as frequency approaches infinity, $A(\omega)$ yields the added mass coefficient matrix in various DoF, $\mu_\infty$. The time-domain representation of the radiation force can be derived as $F_{\text{rad}} = -\mu_\infty \ddot{X} + \tau_{\text{rad}}$.

In irregular seas, the motion response of a rigid floating body in six DoFs ($j,k = \{x,y,z,\phi,\theta,\psi\}$) is obtained by superimposing regular waves with different amplitudes, wavelengths, and propagation directions. The body motions can be evaluated using Eq. (1), by only considering the linear parts, which yields the closed-form relationship, given by Eq. (2), as suggested by Nielsen et al. (2018):

$$-\omega^2(M_{jk} + A_{jk}(\omega))\eta_{ka} + i\omega B_{jk}(\omega)\eta_{ka} + C_{jk}\eta_{ka} = \zeta_a X_j(\omega,\beta), \tag{2}$$

where $M_{jk}$ is the vessel mass, and $A_{jk}$, $B_{jk}$, $C_{jk}$ are the added mass, damping, and restoring components of the hydrodynamic forces, respectively. The second order force, PTO and viscous drag are intentionally removed in the first instance, only to obtain the transfer function of the motions. These terms are later added to the computations to update the response of the object to external non-linear forces. It should be noted that, if the floating object's free surface has a considerable offset due to its station-keeping system, then the mooring and PTO pre-tensions must be included in the restoring matrix at this stage. Otherwise, the transfer function of the final response will not be accurately obtained. The excitation loads are given by $F_j e^{-i\omega t}$, where $F_j$ is the complex amplitude, $\zeta_a$ is the wave amplitude and $e^{-i\omega t}$ is a term involving Euler's formula. For a wave characterized by frequency $\omega$ and direction $\theta$, the excitation load can be represented by the linear equation $F_j e^{-i\omega t} = a\mathcal{X}_j(\omega;\theta)e^{-i\omega t}$, where the load is calculated through linearization of potential forces and integration over the average body surface, based on Bernoulli's equation (Gjeraker, 2021, J.M.J. and Massie, 2001, Faltinsen, 1993). The transfer function describing the amplitude and phase of the body motions relative to the waves is given by Eq. (3):

$$H(\omega,\beta) = \frac{\eta_{ka}}{\zeta_a} = -\omega^2(M + A(\omega)) + i\omega B(\omega) + C^{-1}X_j(\omega,\beta), \tag{3}$$

where the real amplitude operator (RAO) can be obtained by the real part, $|H(\omega,\beta)|$. The complex form of the body motion is introduced as $\eta_k = \eta_{ka}e^{-i\omega t}$. Eq. (3) is a complex number due to the imaginary parts of the motion transfer function associated with the response phase angle. The imaginary part is zero when $i = j$, resulting in a real number cross-spectrum. In this study JONSWAP Spectrum is used for modeling of wave loads. It should be noted that Eq. (3) calculates the response of the floating object in frequency domain, and to estimate this in time domain, sea states can be described by deriving the wave elevation expression for the entire frequency range in wave spectrum. The wave amplitude for component $k$ is estimated by $\zeta_a = \frac{1}{2}\sqrt{S_\zeta(\omega_k)\Delta\omega}$ , where $\zeta_a$ represents the wave amplitude, $S_\zeta(\omega_k)$ denotes the spectral density for frequency $\omega_k$, and $\Delta\omega$ is the frequency interval (Gjeraker, 2021). To account for waves propagating in multiple directions, a spreading function $f(\beta)$ is introduced, representing the 2D wave spectrum as $S_\zeta(\omega,\beta) = S_\zeta(\omega)f(\beta)$ (Gjeraker, 2021). The spreading function $f(\beta)$ allows for the representation of short-crested irregular seas. $\beta$ is the relative direction between object heading and wave direction.

In the context of short-crested irregular seas, the wave elevation is determined by considering both frequency ($\Delta\omega$) and direction ($\Delta\beta$) intervals. This is achieved by summing $N$ spectral components over $M$ directions, as given by Eq. (4) (Nielsen et al., 2018):

$$\zeta = \sum_{k=1}^{N}\sum_{i=1}^{M}\frac{1}{2}\sqrt{2S_\zeta(\omega_k,\beta_i)\Delta\omega\Delta\beta}\cos(\omega_k t + k), \tag{4}$$

where $\zeta$ represents the wave elevation, $S_\zeta(\omega_k,\beta_i)$ is the spectral density for the $k$th frequency component and the $i$th direction, and $t$ is time.

Now, the wave-induced vessel response can be modeled using the RAO derived from Eq. (3) and wave spectrum in the frequency domain for a pair of degrees of freedom (Nielsen et al., 2018):

$$S_{R,ij}(\omega,\beta) = \int_0^\infty H_i(\omega,\beta)H_j^*(\omega,\beta)S_\zeta(\omega,\mu)d\mu, \tag{5}$$

where $i,j = \{x,y,z,\phi,\theta,\psi\}$ represent a pair of the structure DoFs (Nielsen et al., 2018). $H_i(\omega,\beta)$ is the motion transfer function, and $H_j^*(\omega,\beta)$ is its complex conjugate for wave frequency $\omega$ and relative direction $\beta$. $S_\zeta(\omega,\mu)$ represents the two-dimensional wave spectrum.

### 3.1. Wave drift and sum-frequency loads

Estimating wave-induced second-order loads play a significant role in evaluating the design process of WECs, ensuring structural integrity and safety. These loads arise due to the nonlinear interactions between pairs of wave components present in the sea state. Wave drift loads are crucial for understanding the resonance oscillations and mooring fatigue life as they represent low frequency responses. Sum-frequency loads are significant for the dynamic response analysis of the structure in heave, pitch, and roll motions.

The optimal approach for addressing non-linear wave-structure interaction challenges in the hydrodynamic analysis of large floating structures involves leveraging perturbation analysis (Faltinsen, 1993). This technique systematically divides the fluid domain into two distinct regions, utilizing the order of wave amplitudes as a small parameter. The first region encompasses the linear solution, as outlined in the previous section. In the linear solution, the free surface and boundary conditions are satisfied at the mean position of the free surface and the submerged body surface, respectively. Additionally, the fluid pressure and velocity components are linearized up to the first order. The non-linear boundary conditions governing the free surface are taken into account relative to the instantaneous position of the floating body. This adjustment leads to a more precise estimation of pressure distribution, effectively capturing the non-linearities in the velocity of the fluid particles at the free surface.

In this study, the direct pressure integration method is employed for estimating second-order loads. It is important to note that the wave drift loads are directly computed using the solution of first-order potential theory, and the force and moment are correctly evaluated to the second order in wave amplitude, arising from quadratic velocity terms in the Bernoulli's equation (Faltinsen, 1993). The sum-frequency terms obtained through this approach are relatively small, as mentioned by Faltinsen (1993). To enhance accuracy, it is suggested to compute the components of load due to sum-frequency from the second-order potential $\Phi_2$ by solving a boundary value problem with non-homogeneous free surface conditions, thereby imposing a more precise pressure distribution on the free surface (J.M.J. and Massie, 2001).

Unlike first-order wave loads, which are characterized by RAOs applied to individual wave components, second-order wave loads are computed using Quadratic Transfer Functions (QTFs). QTFs operate on paired wave components, defining scaling and phase factors to

ascertain their contributions to the second-order wave load. Therefore, the same approach as the linear solution discussed in the previous section must be followed to predict the stochastic second-order loads on the structures. It can be proven that the diffracted non-linear loads only contribute to Bernoulli's pressure, which can be quantified by integrating the first-order pressure over the structure's surface $F_2 = \iint_S p^{(1)} \cdot \tilde{n}\, dS$.

The first-order pressure $p^{(1)}$ is based on the potential velocity $\phi_1$, which is proportional to $\rho g \cdot \zeta$, where $\zeta$ represents the relative displacement between the wave profile and the body motion. This relationship is represented by $dS = d\zeta \cdot dl$, where $dl$ denotes a differential element along the waterline of the body's surface. The term $\zeta d\zeta$ in the integral creates a quadratic term in the force calculation. Consequently, the wave drift load can be simplified as $F_2 = \frac{1}{2}\int \rho g \zeta^2 \cdot n\, dl$, where $n$ represents the normal vector along the body's surface. This is how the second-order wave amplitude emerges in frequency loads.

Considering a regular wave derived from spectrum analysis: $\zeta^{(1)}(t) = \sum_{i=1}^{\infty} \zeta_i^{(1)} \cdot \cos(\omega_i t + \epsilon_i)$, and substituting it into $F_2$ as described by Faltinsen (1993) and J.M.J. and Massie (2001), the stochastic second-order component of the wave load can be estimated by Eq. (6):

$$F_2(t) = \sum_{i=1}^{N}\sum_{j=1}^{N} \zeta_i^{(1)}\zeta_j^{(1)} P_{ij} \cos((\omega_i - \omega_j)t + (\phi_i - \phi_j)) + \sum_{i=1}^{N}\sum_{j=1}^{N} \zeta_i^{(1)}\zeta_j^{(1)} Q_{ij} \sin((\omega_i - \omega_j)t + (\phi_i - \phi_j)) \quad (6)$$

For the sake of simplifying computations, the high-frequency (sum-frequency) terms are removed from the equation, while the same process must be followed. Note that $P_{ij}$ represents the real (in-phase) part $\Re\left[\mathbf{QTF}(\omega_i, \omega_j)\right]$, while $Q_{ij}$ represents the imaginary (out-of-phase) part, $\Im\left[\mathbf{QTF}(\omega_i, \omega_j)\right]$. These two components constitute the quadratic transfer function, which needs to be computed through the integration of Bernoulli's pressure, as described earlier. The nonlinear loads consists of two QTF variables: wave drift QTFs for difference-frequency load, and sum-frequency QTFs for sum frequency load (Engebretsen et al., 2020). The mean drift force in irregular waves is simply determined by setting $\omega_i = \omega_j$. As described by J.M.J. and Massie (2001), in the frequency domain, the load spectral density of a second-order difference-frequency, denoted by $\Delta\omega$, is given by Eq. (7):

$$S_{F_2}(\Delta\omega) = 8\int_0^{\infty} S_\zeta(\omega) \cdot |S_\zeta(\omega + \Delta\omega)| \cdot |QTF(\omega + \Delta\omega, \omega)|^2 d\omega, \quad (7)$$

where $S_\zeta(\omega)$ represents the spectral density of wave elevation, and the product $S_\zeta(\omega) \cdot S_\zeta(\omega + \Delta\omega)$ contributes to the wave group spectral density (Engebretsen et al., 2020). The QTF function in the integral is comparable to the RAO used in first-order load calculations. Its amplitude is defined as $|QTF(\omega + \Delta\omega, \omega)| = \sqrt{P(\omega + \Delta\omega, \omega)^2 + Q(\omega + \Delta\omega, \omega)^2}$.

### 3.2. PTO system modeling

The APP employs a resilient PTO system which is inspired by the CETO concept, as reviewed by Nielsen et al. (2018), Rijnsdorp et al. (2019) and Tran et al. (2021). The PTO system seamlessly integrates into the floating structure, harnessing energy from the motion of the submerged body. The load in the PTO and their mooring line is fully controlled by the control system, thus not governed by extreme environmental conditions. The technology employs a strategically devised arrangement of multiple moorings, serving as pivotal connection points between the PTO system and the platform. Such configuration facilitates capturing energy not only from vertical heave but also from horizontal surge and rotational pitch. This concept is built upon the notion of finding the trade-off between maximum energy extraction and Survivability.

In this paper, a multi-piecewise linear approach is adopted to simulate the nonlinear behavior of the PTO system. The basis of PTO power output model is an externally-driven nonlinear mechanical oscillator with the equation of motion of $M\ddot{X} + f(X, \dot{X}) = F_{\text{env}}$, where $F_{\text{env}}$ denotes the external force exerted on the PTO, which is a combination of first and second-order wave loads and viscous loads. The internal force $f(X, \dot{X})$ incorporates PTO damping and stiffness effects, and complements the main floating structure body stiffness matrix, presented in Eq. (1). The restoring force is considered as a piecewise linear (PWL) function of displacement $X$ or velocity $\dot{X}$, where both stiffness and damping exhibit linear behavior in each function piece (Nayek et al., 2023). For the sake of simplifying computation, damping effects in the PTO system are neglected. For a PWL stiffness system, the equation of motion becomes $F_{\text{env}} = M\ddot{X} + b_{\text{PTO}}\dot{X} + k_{\text{PTO}}X$, where $b_{\text{PTO}}$ represents the damping coefficient of the PTO system and $k_{\text{PTO}}$ denotes the stiffness coefficient. According to the study by Nayek et al. (2023), two- to four-piece functions are commonly used in attempt to model nonlinear mechanical oscillators. These systems are defined by partitioning the displacement or velocity field into regions of linear operation. In this study, a quadlinear stiffness function is adopted, given by Eq. (8):

$$k_{\text{PTO}}(x) = \begin{cases} k + k_1(x - r_1), & \text{for } x \le r_1 \\ k, & \text{for } r_1 < x \le r_2 \\ k + k_2(x - r_2), & \text{for } r_2 < x \le r_3 \\ k + k_2(r_3 - r_2) + k_3(x - r_3), & \text{for } x > r_3 \end{cases} \quad (8)$$

where, $x$ represents the elongation of the PTO system due to the buoy motion, $k$ is the initial stiffness of the piston. The parameters $r_1$, $r_2$ and $r_3$ denote the thresholds of PTO elongation considered to segment the PTO stiffness into 4 linear sections. The constants $k_1$, $k_2$, and $k_3$ correspond to the slope of stiffness function at each linear section. These parameters play an imperative role in modeling PTO energy output and system integrity; a tighter connection may lead to higher energy absorption but could also induce more forces on the PTO line, increasing the likelihood of failures due to fatigue or overload.

For irregular waves impacting the floating power system, the total power that can be absorbed from a given sea state $s_i$ (in time-domain) within a simulation time of $t_n$ is given by Eq. (9):

$$P_{s_i}(H_s, T_p) = \frac{1}{t_n}\sum_{t=0}^{t_n} \mathbf{F}_{\text{PTO}}(t) \cdot \dot{\mathbf{X}}(t), \quad (9)$$

where $s_i$ is a result of the joint between significant wave height $H_s$ and wave period $T_p$. The force exerted on PTO, $F_{\text{PTO}}$, is determined by directly solving Eq. (1), which involves simultaneously updating the stiffness matrix within the hydrostatic force $F_H$ and the integral for hydrodynamic damping.

Eq. (9) is derived from the conversion of the frequency-domain to time-domain representations, utilizing Eq. (4), (5), and (7). This transformation is performed to enable the evaluation of the hydrodynamic characteristics and power extraction performance of the APP (considering non-linearities and temporal effects). This approach slightly differs from directly multiplying the wave spectrum to power spectrum which results in frequency-domain estimates. The outcome of Eq. (9) can be transformed using fast Fourier transform (FFT), for identifying each frequency's contribution to APP power output. A wavelet transformer is also employed, to better understand the non-linear trends and to determine the time proportion that a frequency is present in a time-series. To determine the average annual power, the power output is multiplied by the matrix indicating the probabilities of various sea states, in conjunction with the matrix containing power values (Tran et al., 2021):

$$P_{\text{avg}} = \sum_{i=1}^{N_s} p_i(H_s, T_p) \times P_{s_i}(H_s, T_p), \quad (10)$$

where $N_s$ represents the number of considered sea states, and $p_i(Hs, Tp)$ is the probability of occurrence of each individual sea state.

### 3.3. Capture width

Capture Width (CW) is a fundamental measure in wave energy assessment. As discussed by Babarit et al. (2012), it expresses the ratio of absorbed wave power ($P_{\text{avg}}$) to the wave resource ($J_{\text{Sea}}$):

$$\text{CW} = \frac{P_{\text{avg}}}{J_{\text{sea}}}, \tag{11}$$

where, $P_{\text{avg}}$ represents the absorbed wave power in kilowatts (kW), here estimated using Eq. (9) and (10). $J_{\text{sea}}$ denotes the available wave resource in kilowatts per meter (kW/m) determined by $J_{\text{sea}} = E \cdot C_g \cdot 1$, where $E = \frac{1}{8}\rho g H^2$, $[J/m^2]$and $C_g = \sqrt{gd}$, [m/s] is group velocity for shallow water, and the multiplication by unity represents unit length of the floating structure. As outlined by Abaei et al. (2017), Eq. (11) has been slightly modified from the original definition provided by Babarit et al. (2012), to allow for direct calculation of the capture length using energy flux. It should be noted that CW is expressed in meters and signifies the width of a wave crest that the WEC effectively captures and harnesses.

## 4. Surrogate model for structural reliability assessment

Given the significant role of fatigue damage in the integrity of WECs, a surrogate model is developed based on structural reliability concepts to evaluate the likelihood of fatigue for the APP design and in various operational conditions. Here, limit state function (LSF) is used to assess whether a component (e.g. mooring line) can still satisfy a specified performance criterion (e.g. bearing hydrodynamic loads). By comparing a load with the capacity of the component (strength threshold), LSF will determine when failure is deemed to occur. To account for the uncertainties associated with operational parameters, they can be described by a random vector $\Theta \in D_\Theta \subset \mathbb{R}$. The fail and safe regions are defined as $D_f$ and $D_s$, respectively, and the component is deemed safe when $\Theta \in D_s$ and failed when $\Theta \in D_f$. The LSF $g(\Theta)$ will generate an $M$-dimensional hypersurface defined by $g(\Theta) = 0$, which delineates the boundary between safe and failure domains (Torre et al., 2021).

The primary objective is to establish a joint probability density function (PDF) for the vector $\Theta$ denoted as $\Theta \sim f_\Theta(\theta)$, which measures the failure probability $P_f = \Pr[g(\Theta) \le 0]$. To quantify the probability of a component failure considering uncertainty in the state parameters, the PDF must be integrated over the failure domain $D_f$, as shown in Eq. (12) (Lemaire, 2013; Torre et al., 2021) :

$$P_f = \int_{D_f} f_\Theta(\theta)d\theta = \int_{\{\theta : g(\theta)\le 0\}} f_\Theta(\theta)d\theta. \tag{12}$$

Estimating $P_f$ directly is rather complex, and a closed-form solution is often only available based on certain assumptions. In practice, it is common to introduce an indicator function $\mathbf{1}_{D_f}(\theta)$, where $\mathbf{1}_{D_f}(\theta) = 1$ if $g(\theta) \le 0$, and $\mathbf{1}_{D_f}(\theta) = 0$ otherwise. Therefore, $P_f$ is defined as $\mathbb{E}[\mathbf{1}_{D_f}(\theta)]$, where $\mathbb{E}[\cdot]$ is the expectation operator associated with the joint distribution of $f_\Theta(\theta)$.

To overcome the challenge of finding closed-form solutions, this paper takes a data-driven approach to solving Eq. (12) based on Bayesian statistics. The Bayesian inference technique is explained in the following sections.

### 4.1. Mooring and PTO fatigue life modeling

In this paper, the fatigue damage growth in the APP mooring and PTO systems is modeled based on the Palmgren–Miner rule (assuming a linear cumulative damage) and S-N curve concepts (DNV, 2015). According to Miner's rule, when the long-term time-series of stress for a component is represented by a stress histogram with a set of constant stress ranges, denoted as $\Delta\sigma_j$, each associated with an observed number of stress cycles in the time-series, $n_i$, occurrence of fatigue failure is determined by Eq. (13) (DNV, 2015):

$$D = \sum_{j=1}^{k} \frac{n_j}{N_j} \le \Delta, \tag{13}$$

Where, $D$ is the accumulated fatigue damage, $k$ is the number of stress ranges, $n_j$ is the Number of observed cycles in stress range $j$, and $N_j$ is the number of constant load cycles in stress range $j$ that lead to failure.

Rainflow counting is adopted to analyze the stress ranges and cycle counts for fatigue damage assessment. The technique is widely used for efficiently analyzing complex stress time histories (Brodtkorb et al., 2000). In selecting the number of stress ranges, ($k$), it is important to ensure sufficient numerical accuracy and avoid loss of information from data. DNV (2015) recommends that a minimum of 20 stress ranges should be included in the analysis, which might result in considerations regarding acquisition of sufficient stress data from an experiment or operation.

Material fatigue resistance tests are frequently carried out using constant-amplitude cyclic loading, and the results are gather in S-N curves which show the number of cycles a specimen can endure at a certain stress level before failure occurs. The equation $N = a_D S^{-m}$ is established to present the relationship between number of cycles $N$ and stress range $S$. A logarithmic transformation of this equation can be used to develop a linear relationship for estimating the cycle numbers to fatigue failure of various materials in offshore applications (DNV, 2015):

$$\log(N) = \log(a_D) - m\log(S), \tag{14}$$

where $a_D$ is the intercept parameter for the S-N curve, and $m$ represents the slope of the S-N curve. For mooring and Power Take-Off (PTO) design, standard rope is widely used as the main material. The value of $a_D$, which is linked to material properties, may introduce uncertainty to the component reliability estimates and must be carefully modeled.

The stress profile of an APP mooring or PTO under tension will be estimated using the time-domain simulation results from Eq. (1), given $\sigma = \frac{F}{A}$, where $F$ is the axial force in mooring line and $A = \pi D^2/4$ is its cross-sectional. Note that the stress profile must theoretically encompass twist and torsion stress; However, for the PTO system and mooring tensioner, where they consistently experience significant axial tension, the influence of these additional contributions is negligible. Rainflow counting is then performed on the obtained stress profile to extract the present stress ranges in data $\Delta\sigma_j$, $j = 1, \dots, k$.

The design fatigue criterion in Eq. (13) is usually set to $\Delta = 1$ in structural reliability assessment; However, this does not always hold and failure might occur at lower values. For more reliable estimation of system design life, the uncertainty of accumulated damage growth must be incorporated into the design process (Liu and Sørensen, 2020; DNV, 2015). The effect of load sequence in variable loading is ignored by the Miner's rule, which can causes error in estimating fatigue damage. Several previous studies showed that using Miner's rule often results in overestimation of fatigue in composite materials (Liu and Sørensen, 2020; Rognin et al., 2009). In the present study, the uncertainty in Miner's rule estimates is dealt with by considering the damage criterion as a random variable with a mean value of less than 1 ($\Delta \sim N(\delta, \Delta\delta)$, $\delta < 1$).

The LSF for fatigue life assessment is then expressed as:

$$g(\Theta, t) = \mathbf{R}(\Theta, t) - \mathbf{L}(\Theta, t), \tag{15}$$

where, $R$ denotes component resistance and $L$ represents load. In this study, a number of time-domain simulations with the time intervals of $t_n$ for different sea states $s_i$ have been used to model long-term exposure of APP to random sea conditions. Considering Eq. (13) and the previous discussions in Section 3, the final form of the fatigue LSF is given by Eq. (16).

$$g(\Theta) = \Delta - D = \Delta - \frac{1}{a_D}\sum_{i=1}^{N_s}\sum_{j=1}^{N_k} \frac{1}{(\Delta\sigma_j)^m} . p_i(H_s, T_p), \tag{16}$$

Note that Eq. (13) has been revised to account for the influence of each modeled sea state in the computation of fatigue damage growth. Additionally, the order of stress range summation is defined as $N_k$, which represents the total number of observed cycles, as $k \cdot n_j$. This simplifies the construction of the LSF given in Eq. (16). For the sake of simplification, Eq. (16) only considers the occurrence probability of sea states, and not the probability of nominal magnitudes (peak-to-trough) of the stress cycles in state $s_i$. The same assumption was previously made by Mozafari et al. (2023) in estimating fatigue life of offshore wind turbine blades. The vector of the stochastic variables in the model is described by $\Theta \sim f(\Delta, a_D, \Delta\sigma_j)$, where the total number of stress cycles $N_k$ is indirectly affected by the results, and will be inherently considered the failure probability estimate.

Predicting the remaining fatigue life ($N_{f,\mathbf{Remain}}$) involves estimating the time before the component (mooring or PTO) reaches the failure threshold (i.e. $\Delta$). This important characteristic is calculated using the linear Eq. (17) (based on Miner's rule):

$$N_{f,\mathbf{Remain}} = t_n \cdot \left(\frac{D_2}{D_1} - 1\right), \tag{17}$$

where, $t_n$ denotes the projected operational exposure time (here, equivalent to the simulation time), $D_1$ is the current status of fatigue damage and $D_2$ at the end of designated exposure time $t_n$. Correspondingly, $D_2 = \Delta$ indicates the threshold associated with failure, a factor recognized as uncertain.

#### 4.1.1. Bayesian inference for fatigue damage prediction

The application of the first order reliability method (FORM) and second order reliability method (SORM) in solving LSFs, although common in structural reliability analyses, is constrained by their limitations. They rely on the Laplace method to approximate the probability of failure with a quadratic function around its mode. As the dimensionality of the problem (specifically the LSF) expands, the accuracy of both approach diminishes necessitating improvements in approximations. The subset simulation (SS) approach gained attention as a alternative solution, yet some studies compared its effectiveness to an asymptotic SORM variant, highlighting its limitations (Breitung, 2021).

In this study, Bayesian inference using the Markov Chain Monte Carlo (MCMC) method is employed as a robust sampling approach estimate the probability of fatigue failure in APP mooring and PTOs. The MCMC simulations dynamically map the failure domain utilizing the LSF $g(\Theta)$. Regardless of the dimensionality of uncertain parameters or the nonlinearity of the failure domain, MCMC offers an effective approach to estimating the failure probability $P_f$ where direct solution is not possible.

Bayesian inference revolves around drawing conclusions based on evidence and has become a cornerstone of modern statistics and machine learning. Its fundamental principle is the Bayes' theorem, given by Eq. (18), which enables the updating of beliefs about some parameters of interest in light of observed data (Gelman et al., 2020):

$$P(\Theta|Y) = \frac{P(Y|\Theta) \cdot P(\Theta)}{P(Y)}, \tag{18}$$

where, $P(\Theta|Y)$ is posterior distribution, which is the updated belief about a collection of random variables $\Theta$ based on the observed data of $Y$. $P(Y|\Theta)$ is the likelihood function, $P(\Theta)$ is the prior distribution and $P(Y)$ is the unconditional likelihood.

The likelihood function $P(Y|\Theta)$ correlates the observed data to unknown parameters $\Theta$, while the prior distribution $P(\Theta)$ represents the prior information about parameters. Here, the parameters $\Theta$ constitute a collection of random variables that shape the uncertainty of the fatigue failure model, as explained in Section 4.1.

For instance, $\Theta$ can include the mean, $\mu$, and standard deviations, $\sigma$, of the distribution representing the stress ranges in mooring lines. In this study, the observed data $Y$ are the time-domain response of moorings and PTOs, which is also a random vector since its values are obtained from various simulations and sea states. Consider $P(Y) = \sum_\Theta P(\Theta)P(Y|\Theta)$, where the summation is taken over all possible values of $\Theta$. To predict fatigue failure using Eq. (12), the model $P(\Theta, Y)$ must first be constructed. This involves MCMC sampling across the failure surface domain $D_\Theta$, as elaborated in Section 4, followed by computing the posterior distribution of the model variables $P(\Theta|Y)$.

In the context of modeling the probability of failure using $g(\Theta)$, the challenge is to identify an appropriate distribution, which the data and consequently the posterior follow. Instead of making assumptions (e.g., based on conventional approaches) which can be crude, this study directly transforms the LSF in Eq. (16) to a logarithmic scale to facilitate Bayesian inference. This approach, often referred to as Incremented Log Density (ILD), proves particularly useful when dealing with unknown shapes of PDFs (Stan, 2020). As outlined by Stan (2020), the ILD process entails employing log probability increment statements within the Bayesian model. This procedure incrementally increases the log density using an expression that characterizes the domain uncertainty (e.g., the function $g(\Theta)$ in this study). For instance, by employing ILD, the log density can be elevated using an expression like $-0.5 \cdot y \cdot y$, where $y$ is a unit normal variable. This methodology can be extended to encompass diverse expressions. The resulting likelihood model can be constructed in this manner, even for situations like drawing a variable from a unit normal distribution: $p(y) = \exp(-y^2/2)/Z$, where $Z$ represents a normalizing constant that guarantees integration to 1, which is not depended on $y$ (Stan, 2020). Consequently, the normal distribution can be efficiently modeled as a quadratic uncertain term $y$, while this approach remains applicable to intricate and unfamiliar expressions such as (16). Utilizing MCMC, the log probability function for real-valued parameters $\Theta$ is evaluated. This function, representing the normalized posterior, forms the basis of Bayesian analysis. The Bayesian inference model components for fatigue life-time are given by Eq. (19):

$$\begin{aligned} a_D, \Delta\sigma_j &\sim \text{Uniform}(a, b), \\ \Delta &\sim N(\delta, \Delta\delta), \\ D|a_D, \Delta\sigma_j &\sim N(\overline{D}, \Delta D), \\ P(g(\Theta)|\Delta, a_D, \Delta\sigma_j) &\sim \sum_\Theta \left(\log(\Delta) - \log(D|\Delta\sigma_{s_i}, a_D)\right), \end{aligned} \tag{19}$$

where, $a_D$ and $\Delta\sigma_j$ are priors with uniform distributions, $\Delta$ is another prior with a normal distribution with a mean of $\delta$ and standard deviation of $\Delta\delta$. Assigning the hyper-parameters $a$ and $b$ requires careful consideration, where excessively wide ranges must be avoided to ensure fatigue life predictions are realistic to what similar studies and standards suggest (DNV, 2015). $D$ is modeled with a normal distribution using a mean of $\overline{D}$ obtained from Eq. (13) and (16) and sampling from aforementioned priors, and a standard deviation of $\Delta D$. The posterior distribution of the failure probability $P(g(\Theta)|\Delta, a_D, \Delta\sigma_j)$ is obtained by accumulating the differences of logarithmic values of $D$ and $\Delta$ (i.e. cumulative damage growth), as shown in Eq. (19). It is important to note that the term $\sum_\Theta$ emphasizes sampling the failure surface across all random variables ($\Theta$). To avoid complexity in the formulation, notations showing variation in exposure time $t_n$ and sea state $s_i$ are neglected; however, their inclusion must be noted by the reader.

It should be noted that the inference model in Eq. (19) generates a set of PDFs for fatigue growth on the entire surface $D_\Theta$. To evaluate failure probability, as described in Eq. (12), the posterior predictive distribution is integrated over the failed domain $D_f$. To this end the posterior predictive distribution enables prediction of the failure probability on the domain by generating the replicating fatigue growth data as $Y_{\text{rep}}$. This distribution is given by Eq. (20), as presented by Gelman et al. (2020):

$$P(Y_{\text{rep}}|Y) = \int_{D_f} p(Y_{\text{rep}}|\Theta) \cdot p(\Theta|Y)\, d\Theta. \tag{20}$$

Therefore the probability of fatigue failure $P_f$ is represented by $p(Y_{\text{rep}}|Y)$, where $Y$ is initial observation which in this study comes

**Table 1**
The APP design and geometric characteristics.

| Parameter | Value | Unit |
|---|---|---|
| **Vessel length** ($L$) | 48.0 | (m) |
| **Vessel width** ($B$) | 10.0 | (m) |
| **Vessel draft** ($D$) | 3.0 | (m) |
| **Mass** ($M$) | 500.0 | (t) |
| **Displacement** ($\Delta$) | 911.4 | ($m^3$) |
| **Center of Mass** ($CoM$) | (2.53, 0.0, −1.97) | (m) |
| **Mass Moment of Inertia, X** ($I_{xx}$) | $1.17 \times 10^6$ | (t $m^2$) |
| **Mass Moment of Inertia, Y** ($I_{yy}$) | $50.0 \times 10^3$ | (t $m^2$) |
| **Mass Moment of Inertia, Z** ($I_{zz}$) | $50.0 \times 10^3$ | (t $m^2$) |

**Table 2**
The APP mooring and PTO line characteristics.

| Parameter | Value | Unit-Reference |
|---|---|---|
| **Weight** ($W_m$) | 0.176 | (kN/m) |
| **Buoyancy** ($B_m$) | 0.131 | (kN/m) |
| **Submerged weight** ($W_{ms}$) | 0.045 | (kN/m) |
| **Min breaking load** ($MBL$) | 3835.5 | (kN) |
| **Intercept parameter of S-N curve** ($a_D$) | $3.4 \times 10^{14}$ | – |
| **Slope of S-N curve** ($m$) | 4.0 | – |
| **Ultimate safety factor** ($SF_{ULS}$) | 1.5 | DNV (2015) |
| **Line diameter** ($d_m$) | 0.15 | (m) |
| **Mooring natural length** ($L_m$) | 90.0 | (m) |
| **PTO natural length** ($L_{PTO}$) | 56.4 | (m) |
| **Axial stiffness (mooring)** ($k_m$) | 326.9 | (kN/m) |

from simulations and the $Y_{\text{rep}}$ are the MCMC sampling from estimated parameters. This means the probability of observing failure damage in future $Y_{\text{rep}}$ (prediction) if the fatigue model produced $Y$ at the current state. The incremental log density function in Eq. (19) and (20) proves valuable outcome not only for real-time fatigue failure modeling, enabling straightforward updating of the likelihood parameter $D$ with sensory data from the environment, but also for extending its utility to implement the variability of mooring assets and operational conditions.

## 5. Case study

### 5.1. APP model and environment setup

In this section, the application of the proposed design evaluation framework is presented in a case study of the APP. The APP model represented a moored floating vessel (4 moorings) and 2 additional lines with PTOs for energy generation. The geometric details of the vessel including its length, width and draft are provided in Table 1. Additionally, the center of mass location is referenced to the origin point (0,0,0) in Orcaflex. The APP is considered to be floating at a water depth of 50 m in a hypothetical site with known sea state conditions. The analyses performed in this paper uses a distribution of wave data, including various significant wave heights $Hs$ and peak wave periods $Tp$. Further details of the sea states used for the analyses are provided later in relevant sections.

At the initial step, an equilibrium analysis is conducted to establish the platform's upright position. This involves defining the initial conditions of the platform, including the pre-tensioning of the mooring lines and PTO systems. The maximum axial stiffness in the mooring lines is considered to be $24 \times 10^3$ kN. Table 2 lists more details on the APP mooring properties. It should be noted that for the purpose of assessing various mooring line tension levels, the studied pre-tension values are provided later in the relevant results section. Table 3 lists the mooring and PTO line connection coordinates including fairlead and anchor points, referenced to the location of vessel center of mass (CoM). To create the PWL stiffness function $k_{\text{PTO}}(x)$, as described in Section 3.2, the PTO is modeled based on 0 to 2 m of elongation (with $r_1 = 0.5$ m, $r_2 2 = 1$ and $r_3 = 1.5$ m) where the axial stiffness slopes are $k = 10$ kN/m, $k_1 = 80$ kN/m, $k_2 = 70$ kN/m, $k_3 = 60$ kN/m.

**Table 3**
The APP mooring arrangements.

| Parameter | Value | Unit |
|---|---|---|
| **Mooring Fairlead** | | |
| **Line 1** | (−14.0, 5.0 , 0.93) | (m) |
| **Line 2** | (−14.0, −5.0 , 0.93) | (m) |
| **Line 3** | (16.8, 5.0 , 0.93) | (m) |
| **Line 4** | (16.8, −5.0 , 0.93) | (m) |
| **Mooring Anchor** | | |
| **Line 1** | (−70.0, 40.0, −51.83) | (m) |
| **Line 2** | (−70.0, −40.0, −51.83) | (m) |
| **Line 3** | (70.0, 40.0, −51.83) | (m) |
| **Line 4** | (70.0, −40.0, −51.83) | (m) |
| **PTO Fairlead** | | |
| **PTO 1** | (25.0 , 4.0 , 0.9) | (m) |
| **PTO 2** | (25.0 , −4.0 , 0.9) | (m) |
| **PTO Anchor** | | |
| **PTO 1** | (40.0, 10.0 , −51.83) | (m) |
| **PTO 2** | (40.0, −10.0 , −51.83) | (m) |

### 5.2. Hydrodynamic loads analysis

As depicted in Fig. 1, the APP concept includes four mooring lines (two at the fore and two at the aft) and two PTO lines at the stern of the vessel. Consequently, the distribution of mooring tensions deviates from conventional moored floating structures. It was observed that this variation introduces distinct pre-tension loads on the system, amplifying stiffness in the yaw direction of the vessel. This enhanced stiffness is necessary to ensure stability, particularly when subject to directional incoming waves. Table 4 presents the optimal APP stiffness matrix (used for estimation of power output) at its upright equilibrium position. The stiffness matrix will vary depending on the pre-tensions applied to the mooring lines and PTOs. This matrix consists of hydrostatic stiffness and static line forces contributing to the line pre-tension, with respect to $F_H$ and $F_{\text{PTO}}$ as defined in Eq. (1). It is important to emphasize that the PTO pre-tensions are dynamically updated according to Eq. (8). Additionally, the buoyancy forces acting on the APP are adjusted to maintain appropriate hydraulic pressure in steady configuration of PTOs.

The analyses of the APP hydrodynamic loads operating at this draft are performed, and the results are presented for each of the three load components (in surge motion) with respect to frequency (see Fig. 2). As it can be seen, the effect of first-order loads consistently surpasses those of the wave drift and sum-frequency. Nonetheless, the second-order loads induce alterations in the structure natural frequency, particularly pronounced in wave drift loads. These changes cause gradually oscillating forces, which can create a pattern of vibration beating phenomenon, reinforcing stress on the mooring system.

To provide a deeper view into the impact of these loads on the APP station-keeping and energy generation systems, the dynamic responses are estimated in time-domain for a range of sea states and pre-tension conditions. The tension time-series from four distinct cases are illustrated in Fig. 3. It is observed from the results that the addition of the two PTOs to the APP structures have caused an uneven distribution of forces in the mooring lines. Consequently, if such arrangement is adopted in a design, PTOs will require adjustments to achieve a balance between the remaining mooring forces and the structural buoyancy.

The most critical tensions are observed in the forward mooring lines (Line 1 and 2). These lines will experience higher loads to ensure the stability of the APP during its operational phases. The average pre-tensions in Line 1 and 2, $T_0$, is used as a reference for each of the cases presented in Fig. 3, only the average pre-tensions, $T_0$ of Line 1 and 2 are mentioned as reference points. These cases represent loads from significant wave height of 1 or 2 m, as the most prevalent sea condition at the Albany site.

**Table 4**
Stiffness matrix of the APP at initial upright equilibrium position (in kN/m).

| wrt global | X | Y | Z | RX | RY | RZ |
|---|---|---|---|---|---|---|
| **X** | **595.17** | −8.98 | 4.68 | 17.24 | 8343.69 | −217.22 |
| **Y** | −8.99 | **361.40** | 5.60 | −2110.75 | −85.58 | −987.85 |
| **Z** | 4.69 | 5.67 | **668.54** | 27.25 | 1285.21 | 69.04 |
| **RX** | 17.21 | −2110.74 | 27.31 | $\mathbf{33.19 \times 10^3}$ | −517.26 | −3178.57 |
| **RY** | 8343.30 | −86.25 | 1285.20 | −528.08 | $\mathbf{272.45 \times 10^3}$ | −1834.12 |
| **RZ** | −217.26 | −987.85 | 68.34 | 8715.12 | −2302.63 | $\mathbf{155.65 \times 10^3}$ |

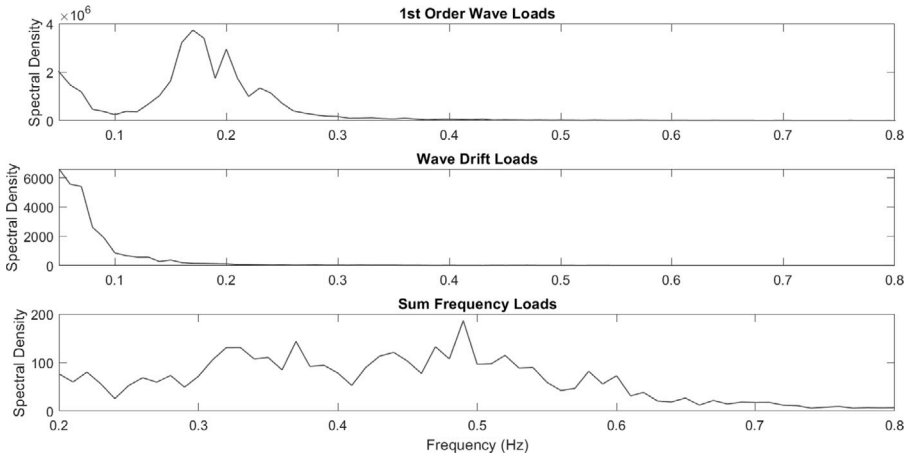


**Fig. 2.** Spectral simulation results of hydrodynamic loads experienced by the APP structure.

The amount of power absorbed by a PTO is highly dependent on the pre-tension imposed on lines 3 and 4. The pre-tension is controlled by the length of the line. The looser these aft mooring lines, the less tolerance against environmental loads. In such condition, more load is transferred to the PTOs resulting in more power generation. However, a softer mooring arrangement will also exert more tension on the forward mooring lines 1 and 2, which increases the risk of failure (overload or fatigue). Therefore, it is an imperative task to design the mooring system for an optimal trade-off between absorbing the highest amount of wave energy and not compromising the integrity of its components. This may present the most significant challenge that the framework developed in this paper is aiming to address.

Fig. 3(a-c) presents three design alternatives (in terms of mooring line pre-tension) including soft, medium and hard options in mooring Lines 3 and 4. Case (d) shows a combination of soft and hard design which means one of the lines in slack and the other in stiff condition. This option seems suitable when the structure is subjected to oblique waves. The results demonstrates that such arrangement provides a substantial opportunity for extracting more wave energy; However, when the main objective is to produce energy at minimum risk of failure, the arrangement is not the most suitable. The remaining of the study will focus on the case with soft mooring lines 3 and 4.

### 5.3. Wave energy output

In this section, the results of assessing the APP performance in harnessing wave energy are presented. As explained previously, time-domain hydrodynamic simulations are conducted for all possible incident waves according to the distribution of wave data observed at the Albany site. The motion response of the PTO and available power at each PTO are estimated using Eq. (19). To evaluate the expected power output, the probability of occurrence for each individual sea state were also (Eq. (10)). The obtained results for the power spectral density (PSD) of each PT (upon performing FFT) is depicted in Fig. 4. The power spectrum shown in Fig. 4 highlights the capability of the APP PTOs in power absorption from a wide range of wave frequencies, though the largest power is expected for wave heights ranging between 1 and 2 m, which is mainly in the wave periods less than 9 s.

To better understand the persistence of power absorption by the APP across various wave periods, continuous wavelet transform (CWT) is performed on the PTO responses. This facilitated the extraction of the frequency–time spectrum during the exposure time denoted as $t_n$ in numerical simulations, ensuring the abrupt changes observed in the output data is accounted for in conversion to frequency-domain. The findings are shown in Fig. 5, where the upper plot illustrates the power spectral density in decibels ($dB$). The color intensity represents the density of the power at each frequency, with warmer colors (e.g., yellow) indicating higher density. It can be seen that there is a significant concentration of power in the lower frequency ranges. This concentration tapers off as frequency exceeds 0.2 Hz. The bottom plot is a spectrogram — the spectrum of frequencies of APP energy output as it varies with time. The color intensity represents the magnitude of CWT (which is proportional and a representative of power) at each frequency and time point. The value of this plot is in the comparison of power output amongst various frequencies and times.

To facilitate a decision-making process that accounts for the uncertainties of decision variables, end-users of this framework will benefit from a probabilistic estimation of available energy. For this reason, empirical PDFs of the APP power output are developed using Eq. (9) and (10), as shown in Fig. 6. Statistical analysis of the results indicate that the expected power that can be captured by the APP is 185 kW, with each PTO contributing to an average of 92.5 kW.

Given the scarcity of WEC structures similar to APP, the CWR calculated using Eq. (11) offers a strong metric for evaluating the viability of the APP concept. According to Babarit et al. (2012), existing WEC technology exhibits CWR values ranging from 6 to 54. Thus, demonstrating that the APP can operate within this range would affirm its potential for power generation. The CWR values for the APP were estimated based on the time domain responses and the histogram presented in Fig. 7. As shown in this figure, the APP model is able to extract wave power with CWR > 6 more than 65% of the time, with an expected value of CWR = 9.5. This confirms that the APP, despite being an emerging multi-purpose offshore platform (MPOP), is comparable to other technologies in harnessing wave energy. This advantage confirms the feasibility of transforming the conventional role of support vessels,

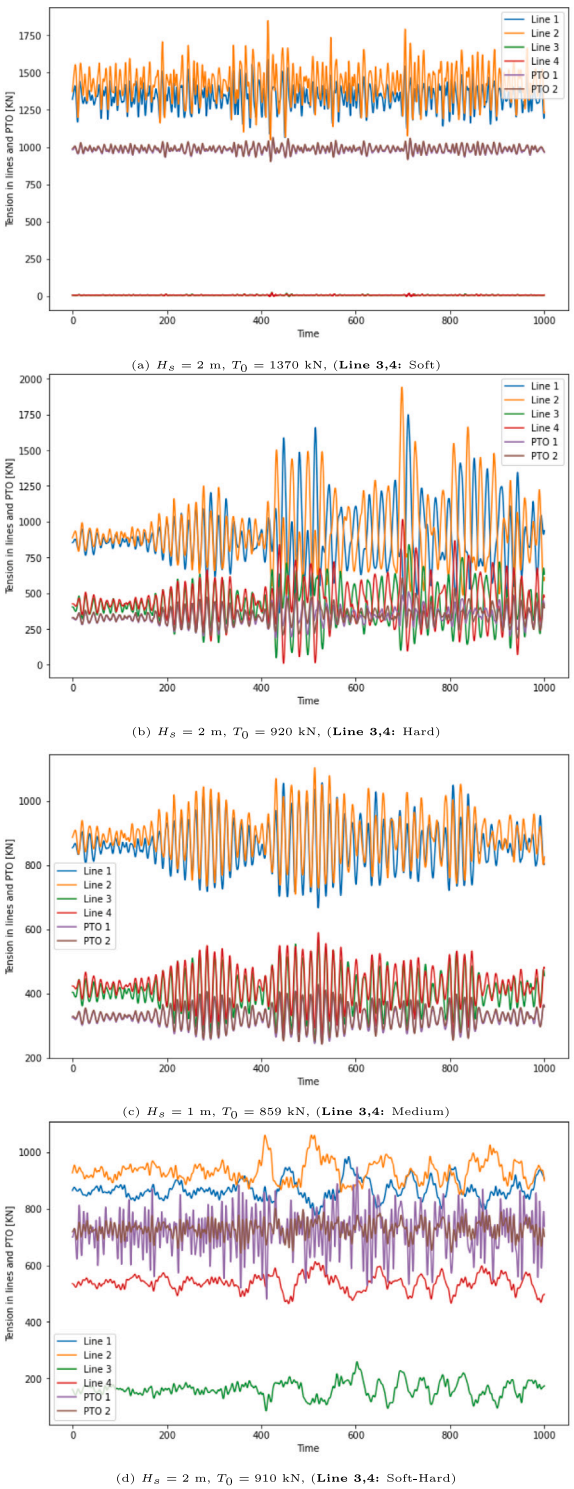


(a) $H_s = 2$ m, $T_0 = 1370$ kN, (**Line 3,4:** Soft)

(b) $H_s = 2$ m, $T_0 = 920$ kN, (**Line 3,4:** Hard)

(c) $H_s = 1$ m, $T_0 = 859$ kN, (**Line 3,4:** Medium)

(d) $H_s = 2$ m, $T_0 = 910$ kN, (**Line 3,4:** Soft-Hard)

**Fig. 3.** Time-series of tension loads on the APP mooring lines and PTOs.

which relied on diesel generators, into a floating aqua power system. Furthermore, Fig. 8 depicts the ability of the APP structure to decrease the amplitude of radiated waves within the shield zone, resulting from the extraction of energy, and provide damping effects to other assets in proximity (e.g., fish pens). The wave profiles shown in Fig. 8 are randomly selected from the time domain response and magnified to highlight the effectiveness of the APP in harnessing wave power within the range of CWR > 6.

**Table 5**
Utilized sea states for results presented in Fig. 9.

| Sea State | $H_s$ (m) | $T_p$ (s) |
|---|---|---|
| **1** | 1.0 | 7.8 |
| **2** | 2.0 | 8.9 |
| **3** | 3.0 | 10.3 |
| **4** | 4.0 | 11.4 |

### 5.4. PTO and mooring fatigue reliability

As discussed earlier, one of the main challenges for ORES is structural deterioration processes (including fatigue) causing failure in components operating under highly random and cyclic loads. Therefore, it is crucial to develop a confident projection of the lifetime of such assets ensuring availability and safety. As recommended by Inspection (2009), risk-based approaches to asset integrity management of floating structures will facilitate continued serviceability and operational integrity. Such practice can also be adopted in evaluation of a design through modeling the deterioration processes based on design parameters and operational conditions.

The framework provided in Section 4 is utilized to evaluate the performance of the APP structure over its lifetime and predict the fatigue damage growth probability in mooring lines and PTO systems. This helps the developers of ORES to optimize their designs for maximum energy generation capability while upholding asset integrity.

The time domain hydrodynamic simulation results for all possible sea states were used to estimate the tensions on the mooring assets, and upon applying the rainflow counting, the stress ranges were defined to input the Miner rule for predicting the fatigue damage growth. The fatigue analysis was performed over an exposure time of $t_n = 1000$, which is deemed sufficient to exhibit trends that can be used for long-term assessment of APP performance. A broader range of load cases with variable sea states were considered to capture all potential responses in the PTO and moorings. In addition to estimating worst-case in each line (maximum damage), a component may experience significantly different damage growths over its geometry (length for mooring lines), especially if the mooring design is a catenary arrangement, as discussed in Section 5.2. For the cases with taut moorings, the damage growth does not vary considerably over the length and they mostly fail near fairleads. In the present case study, Line 3 and 4 are intentionally kept catenary to transfer loads to the PTOs for extracting more energy, which may cause slack loads. It is therefore important to determine the spatial distribution of fatigue growth along the mooring/PTO line. The was performed for the entire mooring system and the results of four cases are presented in Fig. 9. Note that $H_s1.sim$ notation represents the case with a significant wave height of $H_S = 1$ m. As discussed earlier (and shown in Fig. 3), parallel lines manifest very similar responses and for this reason the results from Line 2 and Line 3 are represented by their parallel lines (see Table 5).

The findings indicate that lines 1 and 2 experience much higher fatigue damage growth even in mild environmental conditions, with an expected value of $35.9 \times 10^{-06}$ for $H_s1.sim$. At a dominant wave height of 4 m, the expected damage is expected to reach $8.0 \times 10^{-3}$. Spatially varying fatigue damage in Line 4 is found consistent with the expectations from a catenary arrangement. However, this does not suggest a substantial impact on the APP integrity, as the expected damage is as low as ($< 10 \times 10^{-9}$) even for extreme wave condition ($H_s1.sim$). The results, to some extent, rule out the snap load concerns about mooring fatigues provided sufficient similarity with arrangements in this model. The results presented in Fig. 9 indicated that the PTO lines are expected to have longer life due to a lower fatigue damage (more than 35 years). This validates the feasibility of adopting a catenary arrangement for the design of the mooring lines at the APP stern.

The deterministic representation of structural damage, as provided in Fig. 9, does not account for the occurrence likelihood of each sea

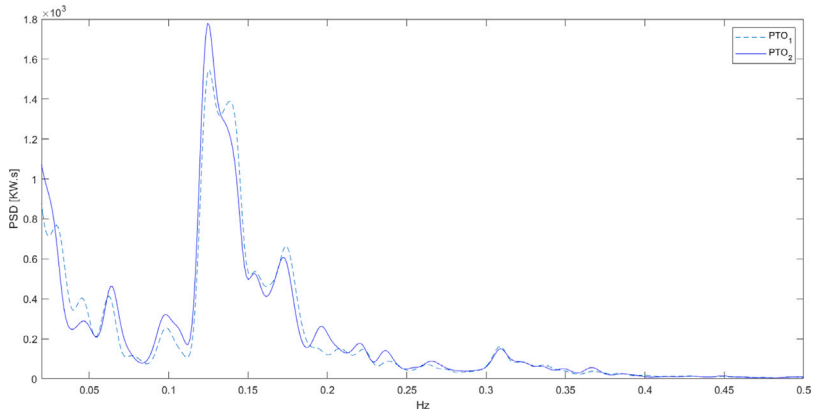


**Fig. 4.** Predicted spectrum of the APP power output for each of its 2 PTOs.

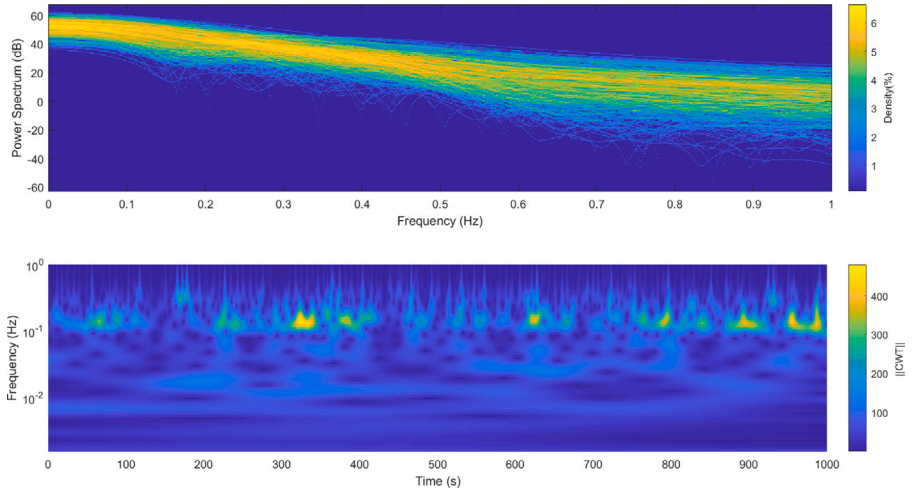


**Fig. 5.** Frequency–time spectrum prediction results of the APP power output.

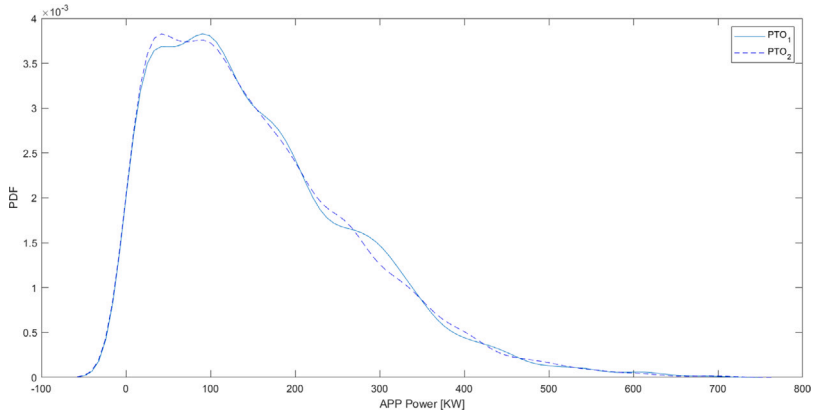


**Fig. 6.** Probability distribution of the expected power output from the APP PTOs.

state. Nevertheless, the significantly high damage growth of 0.01 (for lines 1 & 2 in $H_s1.sim$) underscores a pressing need for continued assessment and monitoring of damage over the asset lifespan. As recommended by DNV (2015), offshore renewable energy structures are typically designed for at least 20-year operational lives, during which the target annual probability of failure of mooring systems should remain below $10^{-5}$ for multiple lines.

The remainder of this section will focus on assessing the fatigue life of mooring Line 1 and 2, as they showed to carry the greatest risk of failure and require careful consideration to enable reliability and robustness in the APP structure design. To address this objective, the mooring tension results were systematically used to derive the LSF, $g(X,t)$. A probabilistic modeling approach was taken in time-domain to predict the probability of mooring failure attributed to fatigue degradation. This analysis considered three distinct operational lives, including 10, 20 and to 30 years to allow for a more classified failure assessment. In this study, four chains were adopted in the MCMC simulations to examine the convergence of the predictions in different scenarios. The

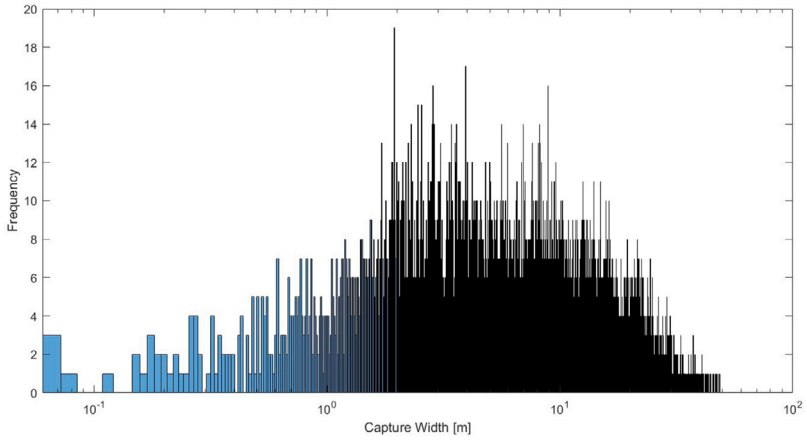


**Fig. 7.** Capture Width (CW) histogram for the APP design.

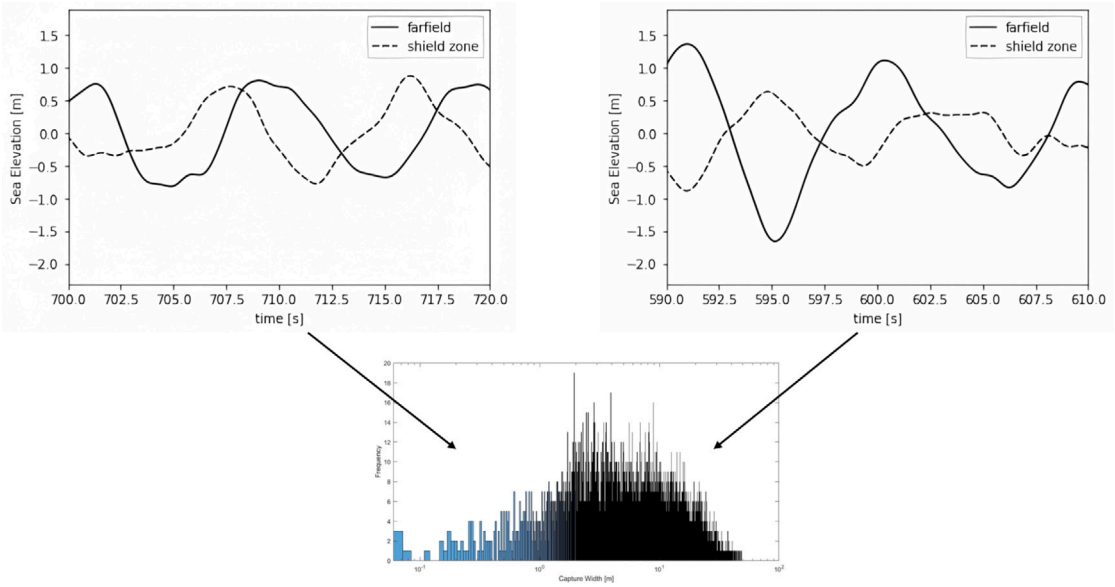


**Fig. 8.** Monitoring the wave profile in the shield zone and far field of the APP structure.

MCMC simulations predict the failure for mooring lines 1 and 2, using the concepts presented in Eq. (19) and (20). The posterior distribution of fatigue damage LSF across the entire domain $D_X = \{D_S, D_f\}$ is shown in Fig. 10. A particularly advantageous aspect of the developed framework is its ability to estimate the posterior distribution of the LSF, which end-users can adopt for computing failure probability depending on their operational limits (failure criterion). It is also important to note that the term $t$ (time) is removed from failure surface (in LSF) as time is now marginalized on the projected design lives in the model (10, 20 and 30 years). The length of time can be readily changed by a developer according to their design.

Next, failure probability $P_f$ is quantified based on the $g(X) < 0$ condition. As it can be seen in Fig. 10, the predicted fatigue damage in the critical moorings of the APP design in this study surpass the recommendations of DNV for fatigue-related failure probability ($P_f < 10^{-5}$). Particularly, for a 10-year design life, the occurrence likelihood of fatigue failure is estimated as $2.8 \times 10^{-18}$. This probability value substantially increases for a 20-year design life, due to non-linear structural deterioration processes, to a cumulative probability fo $P_f = 1.3{\times}10^{-6}$. Although this failure probability is acceptable as per the DNV design guidelines, the projected life expectancy significantly reduces beyond a 10-year operational life, if no interventions are considered. Such interventions may include design improvements or dynamic asset integrity management practices.

Fig. 11(a) presents the MCMC trace plot for the four sampling chains that resulted in failure probability predictions. Fig. 11(b) compares the uncertainty associated with cumulative damage progression over a 10-year life span between Miner's rule results and the MCMC method presented in this paper. The highlighted sections on these probability plots represents potential failure domains, which are distinctively different highlighting the potential overestimation of damage in Miner's rule, as previously suggested by Liu and Sørensen (2020), Rognin et al. (2009).

It is important to highlight that this study also considers the uncertainty linked to the Miner's rule, which can potentially induce additional damage growth in cases where cumulative damage remains below unity. Given the objective of this paper in establishing a robust design evaluation framework for ORES, adopting a conservative stance in the initial stages of concept development may be beneficial to ensure that a design can achieve optimal energy yield and availability. The presented framework has the ability to dynamically monitor the evolving damage patterns and implement real-time adjustments to failure estimations using Eq. (19) and (20). This is achieved by integrating physics-based modeling of the forces and motions with data-driven predictions of structural damage. The approach can be extended to dynamic asset integrity management by utilizing sensory data from field tests or real operations.

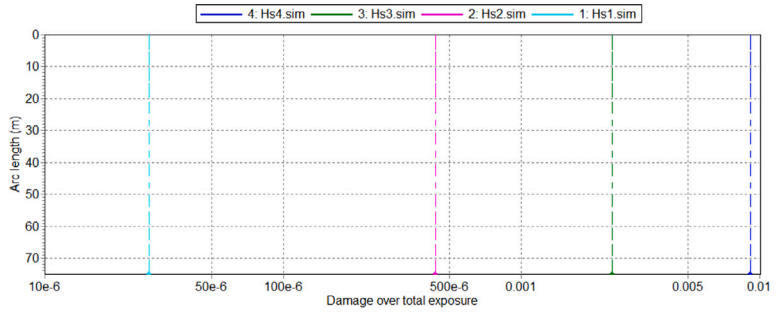


(a) Cumulative Damage in Line 1

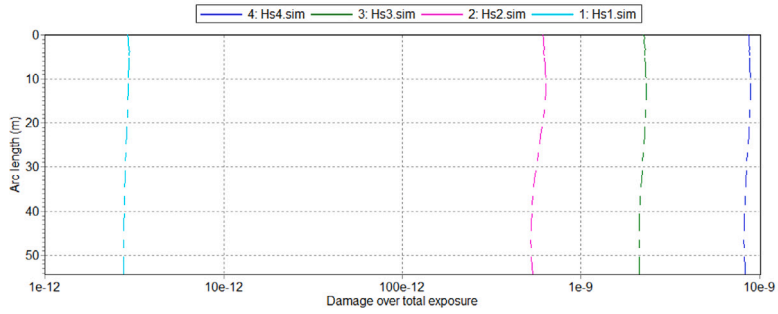


(b) Cumulative Damage in Line 4

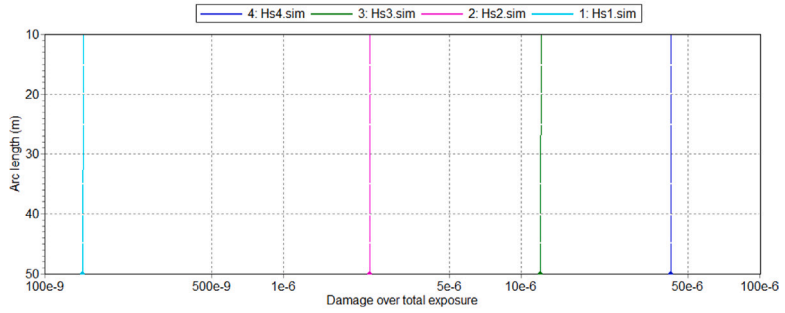


(c) Cumulative Damage in PTO 1

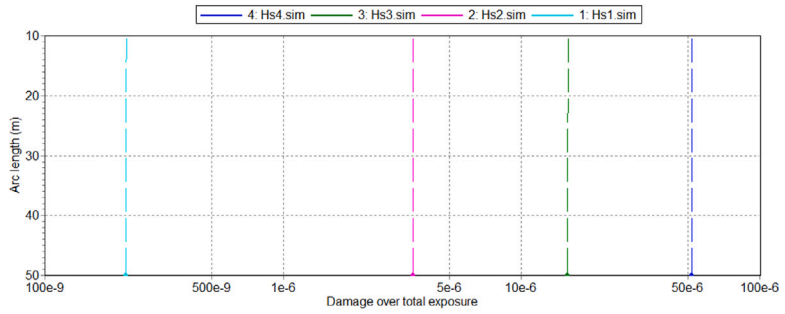


(d) Cumulative Damage in PTO 2

**Fig. 9.** Cumulative fatigue damage growth in mooring lines and PTOs.

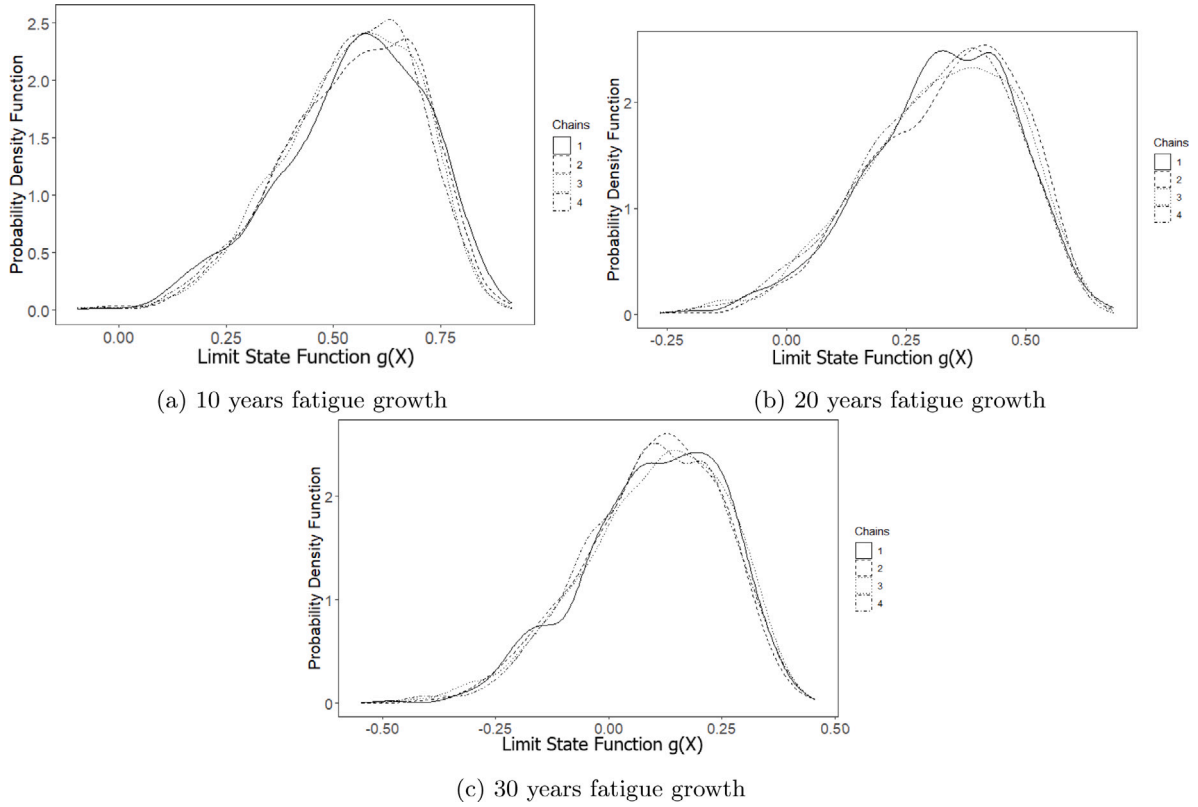


**Fig. 10.** Posterior probability distribution of fatigue damage growth for various design lives (10, 20, 30).

## 6. Conclusion

Offshore aquaculture operations need clean and reliable energy, but face challenges in accessing it. This paper has presented a comprehensive design framework for the APP, a novel WEC concept that integrates a floating platform with a mooring system. The framework has addressed the critical aspects of power generation and structural integrity, including mooring fatigue damage, for the APP. The framework has also introduced a robust surrogate model based on Bayesian data analysis and MCMC to assess the reliability and life cycle of the mooring assets. The framework has been applied to a case study of the APP design and performance, demonstrating its potential as a wave energy solution for offshore aquaculture operations. The paper has also highlighted the importance of management systems, such as Fitness-For-Service Assessment, Integrity Operating Windows, and Management of Change, to ensure the quality and efficiency of the design process and the operation of the APP. The paper has discussed the broader implications of the framework for enhancing the reliability of other offshore energy systems, such as floating wind turbines. The paper has contributed to advancing the feasibility and viability of the APP as a sustainable and efficient wave energy solution for offshore aquaculture operations. The paper has also identified the challenges and opportunities of co-locating WECs and aquaculture structures, and suggested future research directions to optimize mooring layouts and minimize fatigue damages and costs. By addressing these challenges and conducting thorough research, we can advance the effectiveness and viability of wave energy conversion technology and pave the way for sustainable and efficient wave energy solutions.

## CRediT authorship contribution statement

**Mohammad Mahdi Abaei:** Writing – original draft, Validation, Methodology, Formal analysis, Conceptualization. **Ehsan Arzaghi:** Writing – review & editing, Supervision, Methodology, Funding acquisition, Conceptualization. **Minghan Bao:** Validation, Methodology, Formal analysis, Conceptualization. **Vikram Garaniya:** Writing – review & editing, Supervision, Funding acquisition, Conceptualization. **Nagi Abdussamie:** Writing – review & editing, Supervision, Methodology, Funding acquisition, Conceptualization. **Alexandre Pichard:** Writing – review & editing, Funding acquisition, Conceptualization. **Rouzbeh Abbassi:** Writing – review & editing, Funding acquisition, Conceptualization.

## Declaration of competing interest

The authors declare that they have no known competing financial interests or personal relationships that could have appeared to influence the work reported in this paper.

## Acknowledgments

The authors acknowledge the financial support of the Blue Economy Cooperative Research Centre, established and supported under the Australian Government's Cooperative Research Centres Program, grant number CRC-20180101.

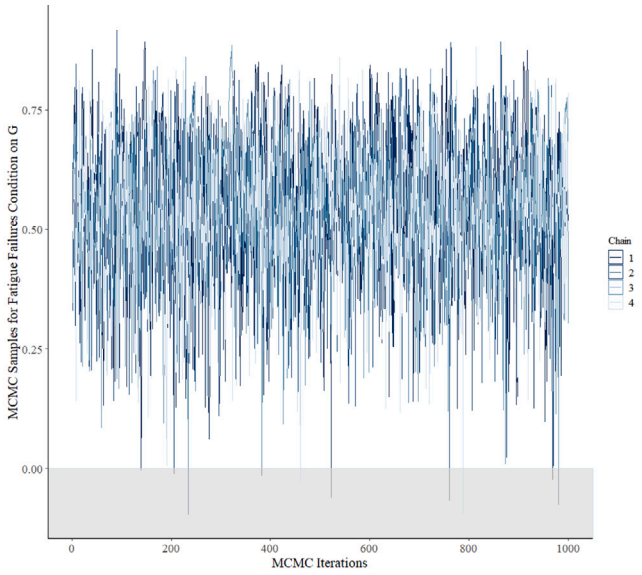


(a) MCMC trace plot for estimating failure domains from limit state function

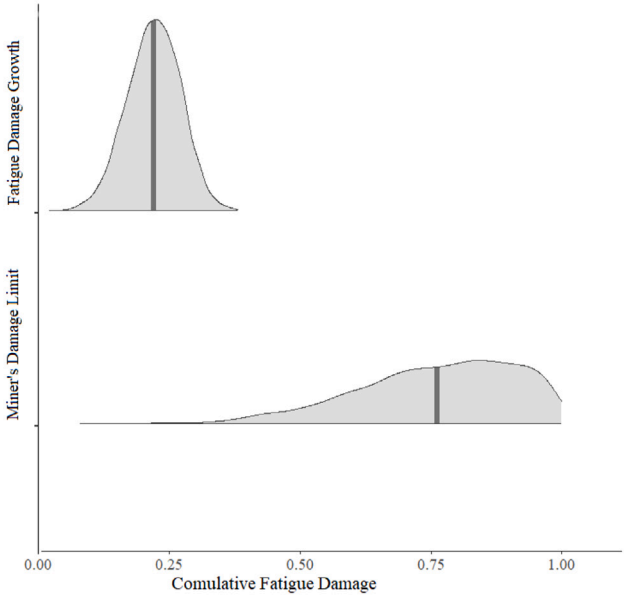


(b) Uncertainty modeling of cumulative fatigue damage

**Fig. 11.** Real time damage progress on mooring lines based on proposed framework.

## References


Abaei, Mohammad Mahdi, Arzaghi, Ehsan, Abbassi, Rouzbeh, Garaniya, Vikram, Penesis, Irene, 2017. Developing a novel risk-based methodology for multi-criteria decision making in marine renewable energy applications. Renew. Energy 102, 341–348. http://dx.doi.org/10.1016/j.renene.2016.10.054.

Al Shami, Elie, Pichard, Alexandre, Cocho, Mathieu, Herran, Miguel Santos, Gough, Ian, 2023. On the survivability of WECs through submergence and passive controllers. In: Proceedings of the European Wave and Tidal Energy Conference, vol. 15.

Babarit, Aurélien, Hals, Jorgen, Muliawan, Made Jaya, Kurniawan, Adi, Moan, Torgeir, Krokstad, Jorgen, 2012. Numerical benchmarking study of a selection of wave energy converters. Renew. Energy 41, 44–63.

Bånkestad, Maria, 2013. Modeling, Simulation and Dynamic control of a Wave Energy Converter. (Master's thesis). Royal Institute of Technology, Stockholm, Sweden.

Breitung, Karl, 2021. FORM/SORM, SS and MCMC: A mathematical analysis of methods for calculating failure probabilities. In: International Probabilistic Workshop. Springer, pp. 353–367.

Brodtkorb, Pär Andreas, Johannesson, Par, Lindgren, Georg, Rychlik, Igor, Rydén, Jesper, Sjö, Eva, 2000. WAFO-a matlab toolbox for analysis of random waves and loads. In: ISOPE International Ocean and Polar Engineering Conference. ISOPE, pp. ISOPE–I.

Carnegie Clean Energy, 2022. "CETO technology". https://www.carnegiece.com/ceto-technology/.

Clemente, D., Rosa-Santos, P., Ferradosa, T., Taveira-Pinto, F., 2023. Wave energy conversion energizing offshore aquaculture: Prospects along the portuguese coastline. Renew. Energy 204, 347–358. http://dx.doi.org/10.1016/j.renene.2023.01.009, URL https://www.sciencedirect.com/science/article/pii/S0960148123000095.

Clemente, D., Rosa-Santos, P., Taveira-Pinto, F., 2021. On the potential synergies and applications of wave energy converters: A review. Renew. Sustain. Energy Rev. 135, 110162. http://dx.doi.org/10.1016/j.rser.2020.110162, URL https://www.sciencedirect.com/science/article/pii/S1364032120304536.

Davidson, Josh, Ringwood, John V., 2017. Mathematical modelling of mooring systems for wave energy converters—A review. Energies 10 (5), http://dx.doi.org/10.3390/en10050666, URL https://www.mdpi.com/1996-1073/10/5/666.

DNV, 2010. Environmental Conditions and Environmental Loads. Det Norske Veritas (DNV).

DNV, G.L., 2015. Offshore Standard: Position Mooring. Technical Report, DNVGL-OS-E301.

Engebretsen, Espen, Pan, Zhiyuan, Fonseca, Nuno, 2020. Second-order difference-frequency loads on FPSOs by full QTF and relevant approximations. In: International Conference on Offshore Mechanics and Arctic Engineering, vol. 84317, American Society of Mechanical Engineers, V001T01A061.

Faltinsen, Odd, 1993. Sea Loads on Ships and Offshore Structures, vol. 1, Cambridge University Press.

FAO, Éd, 2017. Building resilience for food and food security. Rome, Italy FAO.

Faraggiana, Emilio, Chapman, John, Masters, Ian, 2022. Influence of directional wave spreading on a WEC device. Int. Mar. Energy J. 5 (2), 227.

Freeman, MC, Garavelli, L, Wilson, E, Hemer, M, Abundo, ML, Travis, LE, 2022. Offshore aquaculture: a market for ocean renewable energy. Report for Ocean Energy Systems (OES): Lisbon, Portugal.

Gelman, A, Carlin, JB, Stern, HS, Dunson, DB, Vehtari, A, Rubin, DB, 2020. Bayesian Data Analysis. (with Errors Fixed as of 15 February 2021). Chapman and Hall/CRC, Boca Raton, FL, USA.

Gjeraker, Anna Holm, 2021. Response amplitude operator estimation and wave modeling sensitivity. (Master's thesis). NTNU.

Guo, Xinyu, Liu, Zhen, Li, Yulong, Teng, Bin, 2017. Wave attenuation performance of a tautly moored floating breakwater. Ocean Eng. 137, 227–238.

Inspection, Risk-Based, 2009. Api Recommended Practice 580. American Petroleum Institute.

J.M.J., Massie, W.W., 2001. Offshore Hydromechanics. Delft University of Technology.

Kumar, Sumit, Baalisampang, Til, Arzaghi, Ehsan, Garaniya, Vikram, Abbassi, Rouzbeh, Salehi, Fatemeh, 2023. Synergy of green hydrogen sector with offshore industries: Opportunities and challenges for a safe and sustainable hydrogen economy. J. Clean. Prod. 384, 135545. http://dx.doi.org/10.1016/j.jclepro.2022.135545, URL https://www.sciencedirect.com/science/article/pii/S0959652622051198.

Lemaire, Maurice, 2013. Structural Reliability. John Wiley & Sons.

Liu, Y., Sørensen, J.D., 2020. Sensitivity analysis of wind turbine fatigue reliability: effects of design turbulence and the Wöhler exponent. Wind Energy 23 (11), 2304–2318.

Mozafari, Shadan, Dykes, Katherine, Rinker, Jennifer Marie, Veers, Paul, 2023. Effects of finite sampling on fatigue damage estimation of wind turbine components: A statistical study. Wind Eng. 0309524X231163825.

Nayek, R, Abdessalem, AB, Dervilis, N, Cross, EJ, Worden, K, 2023. Identification of piecewise-linear mechanical oscillators via Bayesian model selection and parameter estimation. Mech. Syst. Signal Process. 196, 110300.

Nielsen, Ulrik D., Brodtkorb, Astrid H., Sørensen, Asgeir J., 2018. A brute-force spectral approach for wave estimation using measured vessel motions. Mar. Struct. 60, 101–121.

Pillai, A.C., Chick, J., Johanning, L., 2011. Mooring system design considerations for floating offshore wind turbines. Proc. Inst. Mech. Eng. Part A: J. Power Energy 225 (2), 173–186.

Rijnsdorp, Dirk, Orszaghova, Jana, Skene, David, Wolgamot, Hugh, Rafiee, Ashkan, 2019. Modelling motion instabilities of a submerged wave energy converter. In: Proceedings of the 34th International Workshop on Water Waves and Floating Bodies, Newcastle, Australia. pp. 7–10.

Ringsberg, J.W., Johnson, E., Holmberg, A., Parida, S., 2012. Fatigue assessment of mooring lines for wave energy converters. Ocean Eng. 48, 113–124.

Rognin, F., Abdi, F., Kunc, V., Lee, M., Nikbin, K., 2009. Probabilistic methods in predicting damage under multi-stage fatigue of composites using load block sequences. Procedia Eng. 1 (1), 55–58.

Silva, Dina, Rusu, Eugen, Guedes Soares, C., 2018. The effect of a wave energy farm protecting an aquaculture installation. Energies 11 (8), 2109.

Stan, Development Team, 2020. Stan User's Guide. Stan Development Team, URL https://mc-stan.org/docs/2_25/stan-users-guide/index.html.

Thies, Philipp R., Johanning, Lars, Harnois, Violette, Smith, Helen C.M., Parish, David N., 2014. Mooring line fatigue damage evaluation for floating marine energy converters: Field measurements and prediction. Renew. Energy 63, 133–144. http://dx.doi.org/10.1016/j.renene.2013.08.050, URL https://www.sciencedirect.com/science/article/pii/S0960148113004667.

Torre, E., Marelli, S., Sudret, B., 2021. UQLab user manual–statistical inference. In: Chair of Risk, Safety and Uncertainty Quantification. pp. 4–114.

Tran, N, Sergiienko, NY, Cazzolato, BS, Ding, B, Wuillaume, P-Y, Ghayesh, MH, Arjomandi, M, 2021. On the importance of nonlinear hydrodynamics and resonance frequencies on power production in multi-mode WECs. Appl. Ocean Res. 117, 102924.

Zhang, Yongxing, Zhao, Yongjie, Sun, Wei, Li, Jiaxuan, 2021. Ocean wave energy converters: Technical principle, device realization, and performance evaluation. Renew. Sustain. Energy Rev. 141, 110764. http://dx.doi.org/10.1016/j.rser.2021.110764, URL https://www.sciencedirect.com/science/article/pii/S1364032121000605.